SCIENCE CHINA Materials ARTICLES

mater.scichina.com link.springer.com

Published online 23 October 2019 | https://doi.org/10.1007/s40843-019-1202-x
Sci China Mater 2019, 62(12): 1807–1814

SPECIAL TOPIC: Dedicated to the 70th Birthday of Professor Kenneth R. Poeppelmeier

Non-stoichiometry in $Ca_2Al_2SiO_7$ enabling mixed-valent europium toward ratiometric temperature sensing

Tao Hu[1], Yan Gao[2], Maxim Molokeev[3,4,5], Zhiguo Xia[1*] and Qinyuan Zhang[1*]

ABSTRACT **Eu^{2+}/Eu^{3+} mixed-valence couple co-doped material holds great potential for ratiometric temperature sensing owing to its different electronic configurations and electron-lattice interaction. Here, the correlation of non-stoichiometry in chemical composition, phase structures and luminescence propertis of $Ca_2Al_2Si_{1-x}O_7$:Eu is discussed, and controlled Eu^{2+}/Eu^{3+} valence and tunable emission appear with decreasing Si content. It is found that the $2Ca^{2+} + Si^{4+} \leftrightarrow Eu^{2+} + Eu^{3+} + Al^{3+}$ cosubstitution accounts for the structural stability and charge balance mechanism. Benefiting from the diverse thermal dependent emission behaviors of Eu^{2+} and Eu^{3+}, $Ca_2Al_2Si_{1-x}O_7$:Eu thermometer exhibits excellent temperature sensing performances with the maximum absolute and relative sensitivity being 0.024 K^{-1} (at 303 K) and 2.46% K^{-1} (at 443 K) and good signal discriminability. We propose that the emission quenching of Eu^{2+} is ascribed to 5d electrons depopulation through Eu^{2+}/Eu^{3+} intervalence charge transfer state, while the quenching of Eu^{3+} comes from multi-phonon relaxation. Our work demonstrates the potential of $Ca_2Al_2Si_{1-x}O_7$:Eu for noncontact optical thermometry, and also highlights mixed-valence europium-containing compounds toward temperature sensing.**

Keywords: temperature sensing, phosphor, Eu^{2+}/Eu^{3+}, intervalence charge transfer

INTRODUCTION

Temperature, as one of the basic thermodynamic parameters, determines properties of matters, and affects the way of production and life activities of mankind deeply. Whereas, an accurate temperature measurement for fast-moving objects, micro devices and chemically/thermally harsh environment is still very difficult [1–4]. To solve this problem, optical thermometry based on detecting temperature-sensitive optical parameters such as spectral position, emission intensity, emission band shape, emission bandwidth, fluorescence lifetime and fluorescence intensity ratio (FIR), attracts growing interest due to its high spatial resolution, rapid response, and noninvasivity [5–12]. Benefiting from independence on spectral losses, external interference and fluctuations in excitation density, FIR technique is highly desired among various optical temperature sensing schemes [13–16]. Essentially, the FIR-based temperature sensing is achieved by monitoring two discriminable emission peaks as the signals whose responses to temperature are significantly different. So far, the thermally coupled levels (TCL) of many rare earth ions (such as Er^{3+}: $^4S_{3/2}/^2H_{11/2}$ [17,18]; Ho^{3+}: $^5G_6/^3K_8$ [19,20]; Nd^{3+}: $^4F_{7/2}/^4F_{3/2}$ [21]), and transition metal ions (such as Cr^{3+}: $^2E/^4T_1$ [22,23]), are often utilized as temperature probes. With variation of temperature, electron populations at the lower and upper level of TCL could change oppositely, resulting in varied FIR. However, due to the narrow energy gap between TCL (ΔE < 2000 cm^{-1}), such thermometric strategy is notorious for low relative temperature sensitivity (S_r). Moreover, thermal broadening of the two emission signals at elevated temperature could also lead to an inferior signal discriminability.

To avoid the TCL limitations, many researchers shift

[1] State Key Laboratory of Luminescent Materials and Devices, South China University of Technology, Guangzhou 510641, China
[2] School of Applied Physic and Materials, Wuyi University, Jiangmen 529020, China
[3] Laboratory of Crystal Physics, Kirensky Institute of Physics, Federal Research Center KSC SB RAS, Krasnoyarsk 660036, Russia
[4] Siberian Federal University, Krasnoyarsk 660041, Russia
[5] Department of Physics, Far Eastern State Transport University, Khabarovsk 680021, Russia
[*] Corresponding authors (emails: qyzhang@scut.edu.cn (Zhang Q); xiazg@scut.edu.cn (Xia Z))

their attention to FIR-based dual-emitting-centers with different thermal-dependent emission behaviors [24]. For instance, Eu^{3+}/Tb^{3+} [25], Pr^{3+}/Tb^{3+} [5], Sn^{2+}/Mn^{2+} [26], and Eu^{3+}/Cr^{3+} [27] couples doped materials have been studied as excellent optical thermometric media. Beyond that, Eu^{2+} generally shows a relatively faster emission quenching rate compared with Eu^{3+}, and thus Eu^{2+}/Eu^{3+} mixed-valence couple is also ideal for temperature determination, which can achieve both high sensitivity and excellent signal discriminability [28,29]. Whereas, the formation mechanism of Eu^{2+}/Eu^{3+} coexisting material is unclear. Besides, as for Eu^{2+} quenching in Eu^{2+}/Eu^{3+} co-doped system, e.g., Sc_2O_3:Eu^{2+}/Eu^{3+} [28], researchers explained it as 5d and 4f energy level crossover relaxation. As a matter of fact, mixed-valence lanthanide (Ln) compounds usually exhibit unusual electronic properties that strikingly different from single-ion containing compounds [30,31]. Taking Eu^{2+}/Eu^{3+} as an example, except for the Eu^{3+}: f-f interconfigurational transition lines and broadband Eu^{2+}: f-d transition, there also exists a broad absorption band at the low energy side in the Eu mixed-valence crystals $Na_5Eu_7Cl_{22}$ and KEu_2Cl_6, which is assigned to the Eu^{2+}/Eu^{3+} intervalence charge transfer (IVCT, electron transfer between two metal sites differing only in oxidation state) [31,32]. More recently, Joos *et al.* [33] combined theoretical and experimental studies on Eu-doped CaF_2, SrF_2, and BaF_2, also proving the existence of Eu^{2+}/Eu^{3+} IVCT, and further pointed out that the low lying Eu^{2+}/Eu^{3+} IVCT state can be a virtually nonradiative decay channel for Eu^{2+}. This seems reasonable although more research related to Eu^{2+}/Eu^{3+} IVCT is absent, because, likewise other studies show Ln^{3+}-M^{n+} (M^{n+} = Ti^{4+}, V^{5+}, Nb^{5+}, Ta^{5+}, Mo^{6+} or W^{6+}) IVCT can indeed quench Ln^{3+} luminescence [5,34–40]. As an example on the IVCT effect, even if a small part of Eu^{2+} is oxided into Eu^{3+} in $BaMgAl_{10}O_{17}$:Eu^{2+}, Eu^{2+} suffers serious quenching than one would expect [41]. Moreover, the reduction of Eu^{3+} to Eu^{2+} in β-Sialon:Eu^{2+} renders the phosphor more efficient luminescence [42], which may also support the theory mentioned above. Therefore, an insightful investigation on the local structures of mixed-valent Eu^{2+}/Eu^{3+} couple and emission quenching mechanisms is crucial for the phosphor development toward ratiometric temperature sensing application.

On the basis of above considerations, herein, specially designed $Ca_2Al_2Si_{1-x}O_7$:Eu (x = 0.00, 0.02 and 0.04) compounds were synthesized at reducing atmosphere. It is found that the valence states of Eu are gradually evolved from +2 to +3 with the decreasing of Si content. Owing to the Eu^{2+} photoluminescence interfered by Eu^{2+}/Eu^{3+} IVCT as we analyzed, the Eu^{2+} emission is highly temperature-dependent. Benefiting from the diverse temperature responses between Eu^{2+} and Eu^{3+}, the FIR of Eu^{2+} (550 nm) to Eu^{3+} (703 nm) shows a high temperature sensitivity in the temperature range of 303–443 K. Moreover, since the well separated two emission peaks, high thermometric discriminability is obtained, which demonstrates the potential of $Ca_2Al_2Si_{1-x}O_7$:Eu for noncontact optical thermometry.

EXPERIMENTAL SECTION

Materials and synthesis

Non-stoichiometry $Ca_2Al_2Si_{1-x}O_7$:0.02Eu (x = 0.00, 0.02, 0.04) were synthesized *via* a high temperature solid-state route. The raw materials, $CaCO_3$ (99.9%), Al_2O_3 (99.9%), SiO_2 (99.99%), and Eu_2O_3 (99.99%) and 3 wt% H_2BO_3 (99.9%) as fluxes were weighted and ground together in an agate mortar for 30 min. Then the mixture was transferred into an alumina crucible and calcined under a reducing atmosphere (5% H_2/95% N_2) at 1400°C for 4 h to obtain the final products.

Characterization

Powder X-ray diffraction (XRD) measurements were performed on an Aeris X-Ray Diffractometer (PANalytical Corporation, Netherlands) operating at 40 kV and 15 mA with monochromatized Cu Kα radiation (λ = 1.5406 Å). The Rietveld structure refinements were performed by using TOPAS 4.2 [43]. Electron paramagnetic resonance (EPR) spectra were recorded by an electron paramagnetic resonance EPR spectrometer (Bruker, A300). The photoluminescence (PL), photoluminescence excitation (PLE) spectra and temperature dependent luminescence spectra were detected by a Hitachi F-4600 fluorescence spectrophotometer. The decay curves were measured by an Edinburgh FLS980 fluorescence spectrophotometer.

The electronic structure calculations for $Ca_2Al_2SiO_7$ matrix were carried out with density functional theory framework using the CASTEP code [44]. The Perdew-Burke-Enzerhof form of the generalized gradient approximation (GGA) was applied to treat the exchange correlation effect. The ultra-soft pseudo-potential was employed to describe the electron-ion interactions. The plane-wave basis set cut-off was 450 eV, K-points grind sampling 3 × 3 × 5. And the lattice was optimized before calculations.

RESULTS AND DISCUSSION

The gehlenite, namely $Ca_2Al_2SiO_7$, is crystalized in tet-

ragonal structure with space group $P42_1m$. Cations are found with three types of sites: large eightfold coordinated site occupied by the large cation Ca^{2+} and two types of tetrahedral site: a regular one, where half of Al^{3+} ions are located, and a very distorted one, where Si^{4+} and half of Al^{3+} ions are statistically distributed, as shown in Fig. 1a. The Eu activators are believed to substitute at Ca^{2+} sites, considering their comparable ionic radius. To understand the impact of Si deficiency on phase and crystal structure of $Ca_2Al_2Si_{1-x}O_7$:Eu (x = 0.00, 0.02, 0.04), powder diffraction data were gathered and Rietveld refinement were conducted. As can be seen, all the peaks are indexed by $Ca_2Al_2SiO_7$ (PDF#87-0968) (Fig. S1) and the compounds are proved to be pure. Therefore, this structure was taken as starting model for Rietveld refinement. Site of Ca ion was occupied by Ca/Eu ions with fixed occupation according to suggested chemical formula. Refinements were stable and gave low R-factors (Fig. 1b, Fig. S2a, b, and Table S1). Coordinates of atoms and main bond lengths are shown in Table S2 and Table S3, respectively. The calculated cell volume V, cell parameter a and c of $Ca_2Al_2Si_{1-x}O_7$:Eu increase with increasing x (inset of Fig. 2b), and thus one can conclude that vacancy size in Al2/Si2 site has slightly bigger ion radii in comparison with Si^{4+} ion. Beyond our expectation, with Si deficiencies, the EPR signals originating from EPR-active Eu^{2+} ion is weakened (Fig. 1c), due to the oxidation of Eu^{2+} into Eu^{3+} (Eu^{3+} ion is EPR-inactive). The valence change will be also proved by spectroscopy as discussed below. As for the charge compensation in $Ca^{2+} \leftrightarrow Eu^{3+}$ replacement, the Al^{3+} substitutes at Si^{4+} site can occur when Si content is decreased, which could also lead to cell volume increasing because the radius of Al^{3+} is bigger than that of Si^{4+}. Therefore, the possible replacement mechanism can be suggested as $Ca^{2+} + Si^{4+} \leftrightarrow Eu^{3+} + Al^{3+}$. Additional one is $Ca^{2+} \leftrightarrow Eu^{2+}$. Thus, the overall replacement mechanism is proposed as $2Ca^{2+} + Si^{4+} \leftrightarrow Eu^{2+} + Eu^{3+} + Al^{3+}$ in this system.

Fig. 1d gives the electronic structures of $Ca_2Al_2SiO_7$ matrix. The calculation predicts that $Ca_2Al_2SiO_7$ has an indirect bandgap (E_g) of 4.54 eV, with the conduction band (CB) minimum at G point and valence band (VB) maximum at Z point. The bottom of CB and the top of VB mainly come from Ca-d and O-p orbitals respectively. Noteworthy, the calculated E_g is smaller than the experimental value of ~ 6 eV [45] due to the inherent shortcoming of the DFT calculation. The large bandgap suggests a large energy barrier for the excited Eu^{2+}: 5d electrons thermally ionized into CB.

Room temperature PL and PLE spectra of $Ca_2Al_2Si_{1-x}O_7$:Eu are presented in Fig. 2a, b. It can be seen that both broadband peaks and sharp narrow lines are observed. The broadband peaks in the PLE (λ_{em} = 550 nm) and PL spectra are expected to originate from

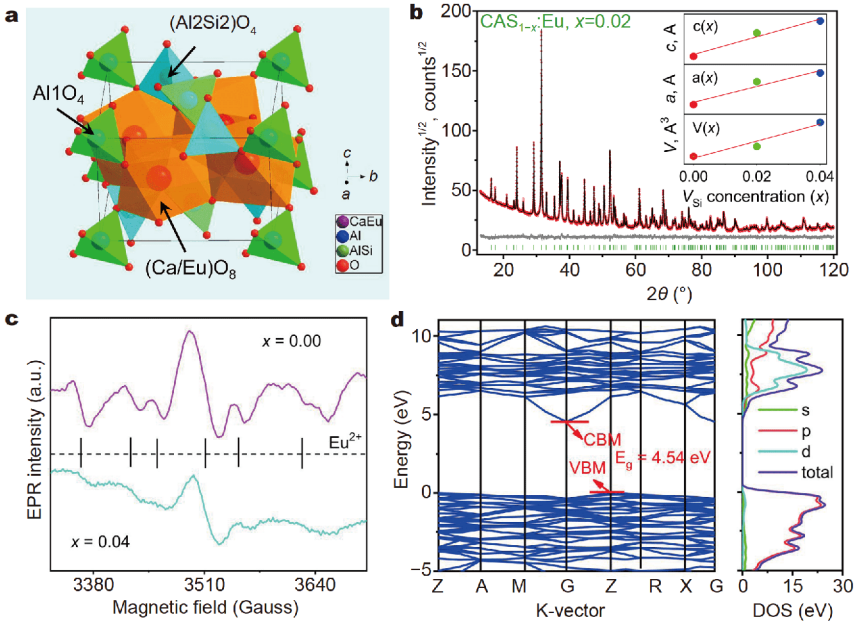

Figure 1 (a) The unit cell of $Ca_2Al_2Si_{1-x}O_7$:Eu structure showing the $Al1O_4$, $(Al2/Si2)O_4$ and Ca/EuO_8 polyhedrons. (b) Difference Rietveld plot of $Ca_2Al_2Si_{1-x}O_7$:0.02Eu, x = 0.02. The inset shows the cell volume V, cell parameters a and c of $Ca_2Al_2Si_{1-x}O_7$:0.02Eu samples as a function of x. (c) EPR spectra of two representative samples (x = 0.00 and 0.04). (d) Calculated electron structure of $Ca_2Al_2SiO_7$ matrix.

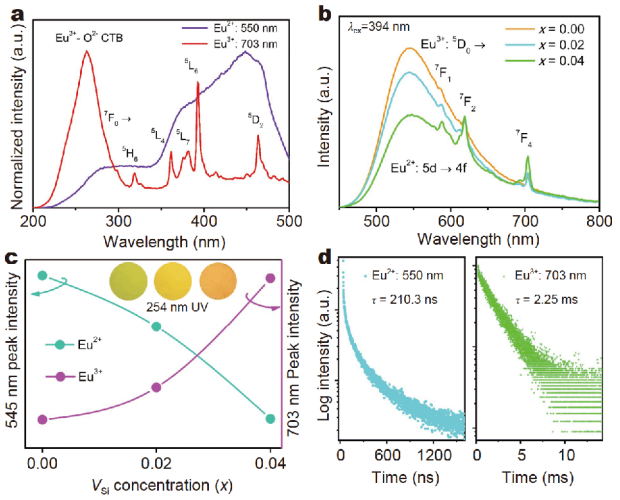

Figure 2 Room temperature (a) PLE spectra (λ_{em} = 550 and 703 nm) and (b) PL spectra (λ_{ex} = 394 nm) of $Ca_2Al_2Si_{1-x}O_7$:Eu (x = 0.00, 0.02, 0.04). (c) 545 and 703 nm peak intensity as a function of x. The inset shows the photographs taken under 254 nm UV light. (d) PL decay curves of Eu^{2+}: 550 nm and Eu^{3+}: 703 nm emission for the sample of $Ca_2Al_2Si_{1-x}O_7$:Eu (x = 0.04).

Eu^{2+}: 4f ↔ 5d transition, while the narrow lines are Eu^{3+}: 4f ↔ 4f transitions. The Eu^{3+} characteristic lines are denoted in the PLE and PL. Those results confirm the coexistence of Eu^{2+} and Eu^{3+} in $Ca_2Al_2Si_{1-x}O_7$. Besides, with x increase, we found that the Eu^{2+} emission was gradually quenched, accompanied by Eu^{3+} emission getting stronger (Fig. 2b, c). Similar phenomena are also observed when the phosphors are excited at 260 nm UV light (Fig. S3). The inset of Fig. 2c shows the digital photographs of the studied samples taken under 254 nm UV light, where the emission color turns from yellow green to orange red as expected. Anyway, all those results give solid evidences of valence change from Eu^{2+} to Eu^{3+}, in line with EPR results. However, it is difficult to determine the Eu^{2+}/Eu^{3+} contents in $Ca_2Al_2Si_{1-x}O_7$:Eu due to the very low doping level (0.02 mmol). It is also worthy to mention that the stoked shift emission of Eu^{2+} is rather small according to the PLE and PL data, and this implies that, the energy barrier for energy level crossover relaxation between 4f and 5d is large. As further confirmed in Fig. 2d, the PL decay time for the broadband emission and the line emission are in nanosecond (210.3 ns) and microsecond (2.25 ms) orders respectively, which are the characteristics of Eu^{2+} electric-dipole allowed 5d → 4f transition and Eu^{3+} electric-dipole forbidden $^5D_0 \rightarrow {}^7F_4$ transition. The lifetime of Eu^{2+} in $Ca_2Al_2Si_{1-x}O_7$ is relatively shorter compared with many other Eu^{2+} doped compounds, which is mainly due to the formation of defects *via* non-stoichiometry substitution and the room temperature quenching of Eu^{2+}, verified by the emission decay lifetime of 0.745 μs measured at 77 K (Fig. S4).

To explore possible application of the phosphor in optical thermometry, the temperature-dependent PL spectra of one typical sample (x = 0.04) are recorded from 303 to 443 K, as presented in Fig. 3a, b. And the histogram of Eu^{2+} (550 nm) and Eu^{3+} (703 nm) emission intensity *versus* temperature (T) is provided in Fig. 3c. As temperature rises, the Eu^{2+} emission (at 550 nm) intensity decreases dramatically, while Eu^{3+} emission (at 703 nm) keeps at almost constant level. As a result, the emission color changes from yellow to orange red, as shown in the Commission International de L'Eclairage (CIE) chromaticity diagram (Fig. 3d), CIE data (Table S4) and digital photograph (inset of Fig. 3d). Consequently, the FIR between the characteristic emissions of Eu^{2+} (550 nm) and Eu^{3+} (703 nm) can be used as temperature measurement index. The measured plots of the FIR *versus* T are illustrated in Fig. 4a. Evidently, it can be well fitted by the exponential formula:

$$\mathrm{FIR} = 79.2\exp(-T/82.2) - 0.182, \tag{1}$$

with a high coefficient of determination (R^2) of 0.997.

The absolute sensitivity S_a, defined as the average FIR change with respect to T, and the relative sensitivity S_r, defined as the rate of FIR changing along with T, can be expressed as [46,47]:

$$S_a = \left|\frac{\partial \mathrm{FIR}}{\partial T}\right|, \tag{2}$$

$$S_r = \left|\frac{\partial \mathrm{FIR}}{\partial T}\frac{1}{\mathrm{FIR}}\right| \times 100\%. \tag{3}$$

The calculated values of S_a and S_r are given in Fig. 4b. The maximum value of S_a is 0.024 K^{-1} (at 303 K) and that of S_r is 2.46% K^{-1} (at 443 K), which is much higher than those of many other reported thermometers, such as $NaGd(MoO_4)_2$:Pr^{3+},Tb^{3+} ($S_{rmax.}$ = 2.05% K^{-1}) [5], La_2MgTiO_6:Pr^{3+} (S_{rmax} = 1.28% K^{-1}) [39], LuNbO4:Pr^{3+}, Tb^{3+} ($S_{amax.}$ = 0.024 K^{-1}, $S_{rmax.}$ = 1.26% K^{-1}) [40], $Ca_6BaP_4O_{17}$:Eu^{2+} ($S_{amax.}$ = 0.011 K^{-1}, $S_{rmax.}$ = 1.53% K^{-1}) [48], and $Na_3Sc_2P_3O_{12}$:Eu^{2+},Mn^{2+} ($S_{rmax.}$ = 1.556% K^{-1}) [49]. Additionally, the energy difference between two emission signals (550 and 703 nm) is about 3960 cm^{-1}, providing a high signal discriminability for temperature detection. All these results indicate that $Ca_2Al_2Si_{1-x}O_7$:Eu is satisfying in the temperature sensing field.

The temperature-dependent PL decay curves are measured to give a further understanding of the diverse thermal PL behaviors among Eu^{2+} and Eu^{3+}. As depicted

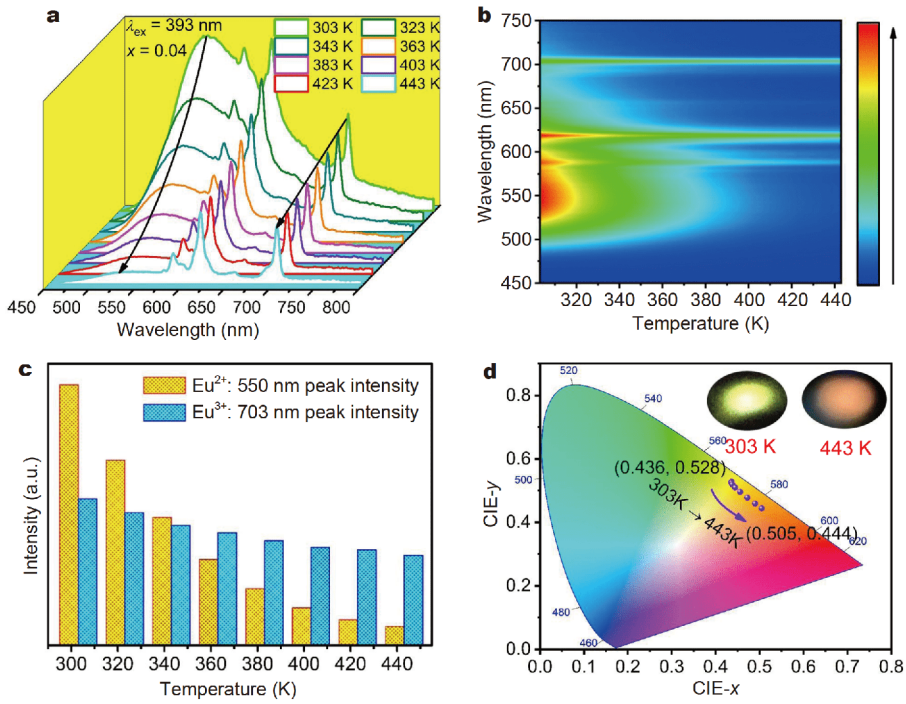

Figure 3 (a, b) Temperature-dependent (303–443 K) PL spectra ((λ_{ex} = 394 nm) of $Ca_2Al_2Si_{1-x}O_7$:Eu (x = 0.04)). (c) Histogram displaying the Eu^{2+} emission intensity (550 nm) and Eu^{3+} emission intensity (703 nm) *versus* recording temperature. (d) CIE (x, y) coordinate diagram of the emission colors at various temperature. The insets are the photos of the sample under 394 nm UV excitation, taken at 303 and 443 K, respectively.

in Fig. 5a, b, totally different temperature-dependent decay behaviors are observed, with Eu^{2+} lifetimes greatly shorten while Eu^{3+} lifetimes slightly declined along with temperature. Based on the temperature-dependent PL spectra and PL decay curves, the thermal quenching temperature for Eu^{2+}, $T_{50\%}$, is roughly estimated at ~330 K, which is far below than that of the majority of Eu^{2+} activated phosphors [50]. The fluorescence lifetimes in the temperature range of 323–443 K can be fitted by the Struck-Fonger theoretical model [51]:

$$\tau(T) = \frac{\tau_0}{1 + A\exp(-\Delta E_1 / k_B T)}, \quad (4)$$

where, $\tau(T)$ is the fluorescence lifetime at a given temperature, τ_0 is the fluorescence lifetime at 0 K, k_B is the Boltzmann constant, and A is the pre-exponential constant. By fitting (R^2 = 0.995), the thermal activation energy ΔE_1 is determined to be around 1853 cm^{-1}.

The possible thermal quenching mechanism behind the Eu^{2+}/Eu^{3+} mixed-valence co-activated $Ca_2Al_2Si_{1-x}O_7$ is schematically illustrated in Fig. 6. Commonly, there are two widely accepted mechanisms responsible for the thermal quenching route of Eu^{2+}, namely, thermal ionization and thermally induced 4f and 5d level intersystem crossover relaxation. However, both of the two processes are hard to occur in present case, because it should overcome a large energy barrier as we analyzed above, yet a relative low temperature of 330 K cannot afford such energy. Therefore, we tentatively ascribe the thermal quenching of Eu^{2+} to the low lying Eu^{2+}/Eu^{3+} IVCT state in $Ca_2Al_2Si_{1-x}O_7$, i.e., the electrons that pumped at Eu^{2+}: 5d state can easily overcome 1853 cm^{-1} energy barrier and then depopulate through IVCT state, resulting in Eu^{2+} emission quenching. As a comparison, the quenching of Eu^{3+} ion is realized *via* multi-phonon relaxation (MPR) as a consequence of Eu^{3+} interconfigurational transitions belonging to weak ion-lattice coupling. It follows the energy-gap law [52]:

$$A_{nr} = A_{nr}(0)e^{-\alpha \Delta E_2}, \quad (5)$$

where $A_{nr}(0)$ and α are constants depending on the host material, ΔE_2 is the energy gap between the excited state and the next lower state. The energy difference ΔE_2 between $^5D_0$ and $^7F_6$ of Eu^{3+} is about 11,400 cm^{-1}. While, the maximum phonon energy of $Ca_2Al_2SiO_7$ is about ~1020 cm^{-1} [53], which indicates at least eleven effective phonons are required to bridge ΔE_2 energy gap. Therefore, the thermal quenching probability of Eu^{3+} is quite low within the studied temperature range, as shown in the

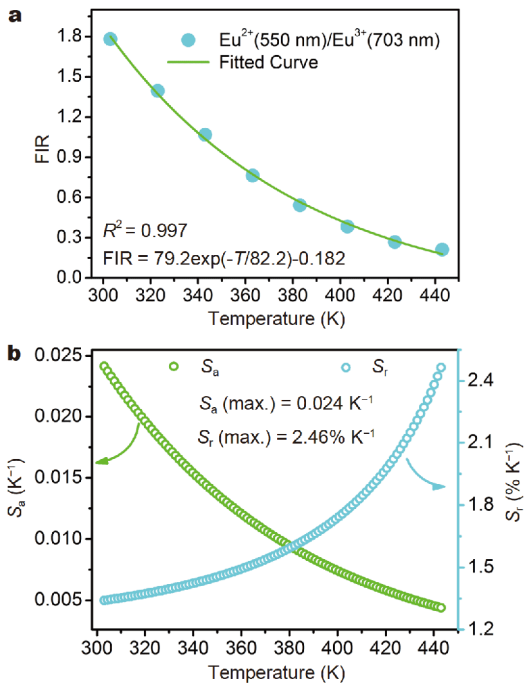

Figure 4 (a) Experiment and fitted plot of FIR of Eu^{2+}(550 nm)/Eu^{3+} (703 nm) *versus* temperature. (b) Absolute sensitivity S_a and relative sensitivity S_r *versus* temperature.

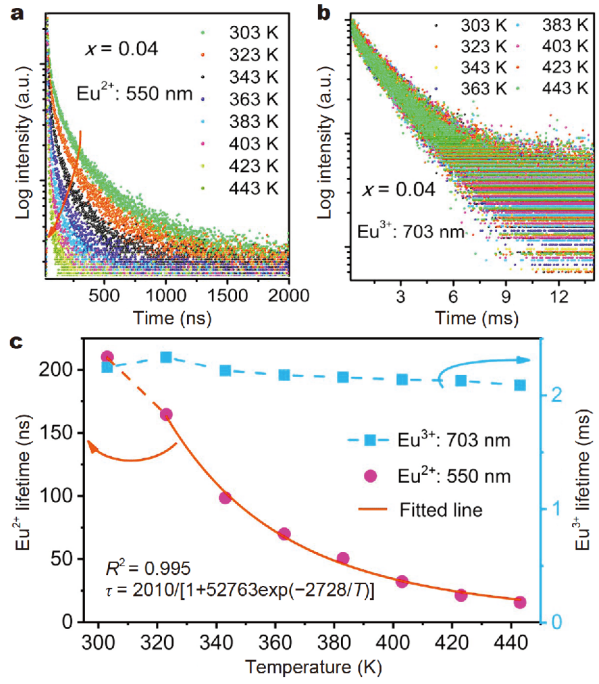

Figure 5 Temperature-dependent fluorescence decay curves of (a) Eu^{2+}: $5d_1$ by monitoring at 550 nm emission, and (b) Eu^{3+}: $^7F_4$ by monitoring at 703 nm emission. (c) The fluorescence lifetime of Eu^{2+}: 5d and Eu^{3+}: $^7F_4$ *versus* temperature.

Eu^{3+} temperature-dependent fluorescence decay curves (Fig. 5 b).

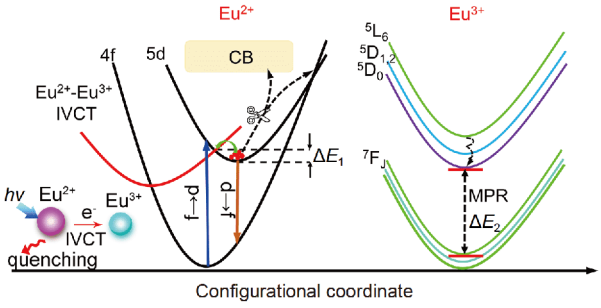

Figure 6 Schematic configurational coordinate diagrams for Eu^{2+} and Eu^{3+}, showing the PL thermal-sensitivity mechanisms.

CONCLUSIONS

In summary, the Eu^{2+}/Eu^{3+} mixed-valence couple doped $Ca_2Al_2Si_{1-x}O_7$ (x = 0.00, 0.02, 0.04) phosphors were successfully prepared under the reducing atmosphere. With the Si-deficiency, the valence state of Eu was gradually changed from +2 to +3, probably accompanied by Al^{3+} ions substitution at Si^{4+} sites. Benefiting from the diverse thermal response emission behaviors of Eu^{2+} and Eu^{3+} in this $Ca_2Al_2Si_{1-x}O_7$ host, the FIR of Eu^{2+} to Eu^{3+} is highly temperature sensitive in the temperature range of 303–443 K. As a consequence, the phosphor exhibits high temperature sensing performance with the maximum absolute and relative sensitivity being 0.024 K^{-1} (at 303 K) and 2.46% K^{-1} (at 443 K), respectively. Moreover, the two characteristic emission peaks of Eu^{2+} (at 550 nm) and Eu^{3+} (at 703 nm) are well separated, providing a good signal discriminability for temperature sensing. The Eu^{2+} and Eu^{3+} thermal quenching mechanisms are analyzed within the framework of configurational coordinate diagram. We propose that the dramatic thermal quenching of Eu^{2+} luminescence is probably induced by Eu^{2+}/Eu^{3+} intervalence charge transfer state. This work demonstrates a novel and an excellent self-calibrated temperature sensing material.

Received 27 August 2019; accepted 30 September 2019; published online 23 October 2019

1 Vetrone F, Naccache R, Zamarrón A, *et al.* Temperature sensing using fluorescent nanothermometers. ACS Nano, 2010, 4: 3254–3258

2 Fischer LH, Harms GS, Wolfbeis OS. Upconverting nanoparticles for nanoscale thermometry. Angew Chem Int Ed, 2011, 50: 4546–

4551
3 Dong B, Cao B, He Y, *et al.* Temperature sensing and *in vivo* imaging by molybdenum sensitized visible upconversion luminescence of rare-earth oxides. Adv Mater, 2012, 24: 1987–1993
4 McLaurin EJ, Vlaskin VA, Gamelin DR. Water-soluble dual-emitting nanocrystals for ratiometric optical thermometry. J Am Chem Soc, 2011, 133: 14978–14980
5 Gao Y, Huang F, Lin H, *et al.* A novel optical thermometry strategy based on diverse thermal response from two intervalence charge transfer states. Adv Funct Mater, 2016, 26: 3139–3145
6 Zhong J, Chen D, Peng Y, *et al.* A review on nanostructured glass ceramics for promising application in optical thermometry. J Alloys Compd, 2018, 763: 34–48
7 Wang X, Wolfbeis OS, Meier RJ. Luminescent probes and sensors for temperature. Chem Soc Rev, 2013, 42: 7834–7869
8 Wang X, Liu Q, Bu Y, *et al.* Optical temperature sensing of rare-earth ion doped phosphors. RSC Adv, 2015, 5: 86219–86236
9 Khalid AH, Kontis K. Thermographic phosphors for high temperature measurements: principles, current state of the art and recent applications. Sensors, 2008, 8: 5673–5744
10 Someya S, Li Y, Ishii K, *et al.* Combined two-dimensional velocity and temperature measurements of natural convection using a high-speed camera and temperature-sensitive particles. Exp Fluids, 2011, 50: 65–73
11 Ji Z, Cheng Y, Cui X, *et al.* Heating-induced abnormal increase in Yb^{3+} excited state lifetime and its potential application in lifetime luminescence nanothermometry. Inorg Chem Front, 2019, 6: 110–116
12 Cheng Y, Gao Y, Lin H, *et al.* Strategy design for ratiometric luminescence thermometry: circumventing the limitation of thermally coupled levels. J Mater Chem C, 2018, 6: 7462–7478
13 Du P, Luo L, Yu JS. Tunable color upconverison emissions in erbium(III)-doped BiOCl microplates for simultaneous thermometry and optical heating. Microchim Acta, 2017, 184: 2661–2669
14 Shi R, Ning L, Huang Y, *et al.* $Li_4SrCa(SiO_4)_2$:Eu^{2+}: A potential temperature sensor with unique optical thermometric properties. ACS Appl Mater Interfaces, 2019, 11: 9691–9695
15 Wang C, Lin H, Xiang X, *et al.* $CsPbBr_3$/$EuPO_4$ dual-phase devitrified glass for highly sensitive self-calibrating optical thermometry. J Mater Chem C, 2018, 6: 9964–9971
16 Cui M, Wang J, Li J, *et al.* An abnormal yellow emission and temperature-sensitive properties for perovskite-type Ca_2MgWO_6 phosphor *via* cation substitution and energy transfer. J Lumin, 2019, 214: 116588
17 Huang F, Yang T, Wang S, *et al.* Temperature sensitive cross relaxation between Er^{3+} ions in laminated hosts: a novel mechanism for thermochromic upconversion and high performance thermometry. J Mater Chem C, 2018, 6: 12364–12370
18 Du P, Yu JS. Synthesis of Er(III)/Yb(III)-doped BiF_3 upconversion nanoparticles for use in optical thermometry. Microchim Acta, 2018, 185: 237
19 Zhou S, Jiang S, Wei X, *et al.* Optical thermometry based on upconversion luminescence in Yb^{3+}/Ho^{3+} co-doped $NaLuF_4$. J Alloys Compd, 2014, 588: 654–657
20 Xu W, Zhao H, Li Y, *et al.* Optical temperature sensing through the upconversion luminescence from Ho^{3+}/Yb^{3+} codoped $CaWO_4$. Sens Actuat B-Chem, 2013, 188: 1096–1100
21 Huang P, Zheng W, Tu D, *et al.* Unraveling the electronic structures of neodymium in $LiLuF_4$ nanocrystals for ratiometric temperature sensing. Adv Sci, 2019, 6: 1802282
22 Back M, Trave E, Ueda J, *et al.* Ratiometric optical thermometer based on dual near-infrared emission in Cr^{3+}-doped bismuth-based gallate host. Chem Mater, 2016, 28: 8347–8356
23 Chen D, Chen X, Li X, *et al.* Cr^{3+}-doped $Bi_2Ga_4O_9$-$Bi_2Al_4O_9$ solid-solution phosphors: crystal-field modulation and lifetime-based temperature sensing. Opt Lett, 2017, 42: 4950–4953
24 McLaurin EJ, Bradshaw LR, Gamelin DR. Dual-emitting nanoscale temperature sensors. Chem Mater, 2013, 25: 1283–1292
25 Cui Y, Song R, Yu J, *et al.* Dual-emitting MOF⊃dye composite for ratiometric temperature sensing. Adv Mater, 2015, 27: 1420–1425
26 Gao Y, Cheng Y, Huang F, *et al.* Sn^{2+}/Mn^{2+} codoped strontium phosphate ($Sr_2P_2O_7$) phosphor for high temperature optical thermometry. J Alloys Compd, 2018, 735: 1546–1552
27 Chen D, Wan Z, Liu S. Highly sensitive dual-phase nanoglass-ceramics self-calibrated optical thermometer. Anal Chem, 2016, 88: 4099–4106
28 Pan Y, Xie X, Huang Q, *et al.* Inherently Eu^{2+} /Eu^{3+} codoped Sc_2O_3 nanoparticles as high-performance nanothermometers. Adv Mater, 2018, 30: 1705256
29 Chen D, Xu M, Liu S, *et al.* Eu^{2+}/Eu^{3+} dual-emitting glass ceramic for self-calibrated optical thermometry. Sens Actuat B-Chem, 2017, 246: 756–760
30 Prassides K. Mixed Valency Systems: Applications in Chemistry, Physics and Biology. Dordrecht: Kluwer, 1991
31 Wickleder C. A new mixed valent europium chloride: $Na_5Eu_7Cl_{22}$. Z für Naturforschung B, 2002, 57: 901–907
32 Wickleder C. KEu_2Cl_6 and $K_{1,6}Eu_{1,4}Cl_5$: Two new mixed-valent europium chlorides. Z anorg allg Chem, 2002, 628: 1815–1820
33 Joos JJ, Seijo L, Barandiarán Z. Direct evidence of intervalence charge-transfer states of Eu-doped luminescent materials. J Phys Chem Lett, 2019, 10: 1581–1586
34 Blasse G. Optical Electron Transfer Between Metal Ions and Its Consequences. Complex Chemistry. Heidelberg: Springer, 1991: 153–187
35 Boutinaud P, Putaj, P, Mahiou R, *et al.* Quenching of lanthanide emission by intervalence charge transfer in crystals containing closed shell transition metal ions. Spectr Lett, 2007, 40: 209–220
36 DeLosh RG, Tien TY, Gibbons EF, *et al.* Strong quenching of Tb^{3+} emission by Tb–V interaction in YPO_4–YVO_4. J Chem Phys, 1970, 53: 681–685
37 Gao Y, Cheng Y, Hu T, *et al.* Broadening the valid temperature range of optical thermometry through dual-mode design. J Mater Chem C, 2018, 6: 11178–11183
38 Gao Y, Huang F, Lin H, *et al.* Intervalence charge transfer state interfered Pr^{3+} luminescence: A novel strategy for high sensitive optical thermometry. Sensor Actuat B-Chem, 2017, 243: 137–143
39 Shi R, Lin L, Dorenbos P, *et al.* Development of a potential optical thermometric material through photoluminescence of Pr^{3+} in La_2MgTiO_6. J Mater Chem C, 2017, 5: 10737–10745
40 Wu Y, Suo H, Zhao X, *et al.* Self-calibrated optical thermometer $LuNbO_4$:Pr^{3+}/Tb^{3+} based on intervalence charge transfer transitions. Inorg Chem Front, 2018, 5: 2456–2461
41 Amidani L, Korthout K, Joos JJ, *et al.* Oxidation and luminescence quenching of europium in $BaMgAl_{10}O_{17}$ blue phosphors. Chem Mater, 2017, 29: 10122–10129
42 Li S, Wang L, Tang D, *et al.* Achieving high quantum efficiency narrow-band β-Sialon:Eu^{2+} phosphors for high-brightness LCD backlights by reducing the Eu^{3+} luminescence killer. Chem Mater, 2017, 30: 494–505
43 Topas V. 1: General profile and structure analysis software for

powder diffraction data. Bruker AXS, Karlsruhe, Germany, 2008
44 Clark SJ, Segall MD, Pickard CJ, *et al.* First principles methods using CASTEP. Z Kristallogr, 2005, 220: 567-570
45 Teixeira VC, Montes PJR, Valerio MEG. Structural and optical characterizations of $Ca_2Al_2SiO_7$:Ce^{3+},Mn^{2+} nanoparticles produced *via* a hybrid route. Optical Mater, 2014, 36: 1580–1590
46 Wang J, Lin H, Cheng Y, *et al.* A novel high-sensitive upconversion thermometry strategy: Utilizing synergistic effect of dual-wavelength lasers excitation to manipulate electron thermal distribution. Sens Actuat B-Chem, 2019, 278: 165–171
47 Cui X, Cheng Y, Lin H, *et al.* Towards ultra-high sensitive colorimetric nanothermometry: Constructing thermal coupling channel for electronically independent levels. Sens Actuat B-Chem, 2018, 256: 498–503
48 Zhou R, Liu C, Lin L, *et al.* Multi-site occupancies of Eu^{2+} in $Ca_6BaP_4O_{17}$ and their potential optical thermometric applications. Chem Eng J, 2019, 369: 376–385
49 Zhang X, Zhu Z, Guo Z, *et al.* A ratiometric optical thermometer with high sensitivity and superior signal discriminability based on $Na_3Sc_2P_3O_{12}$:Eu^{2+},Mn^{2+} thermochromic phosphor. Chem Eng J, 2019, 356: 413–422
50 Qiao J, Xia Z, Zhang Z, *et al.* Near UV-pumped yellow-emitting $Sr_9MgLi(PO_4)_7$:Eu^{2+} phosphor for white-light LEDs. Sci China Mater, 2018, 61: 985–992
51 Struck CW, Fonger WH. Thermal quenching of Tb^{+3}, Tm^{+3}, Pr^{+3}, and Dy^{+3} $4f^n$ emitting states in La_2O_2S. J Appl Phys, 1971, 42: 4515–4516
52 Blasse G, Grabmaier BC. Luminescence Materials. Berlin: Springer-Verlag, , 1994
53 Simondi-Teisseire B, Viana B, Lejus AM, *et al.* Spectroscopic properties and laser oscillation of Yb:Er:$Ca_2Al_2SiO_7$ in the 1.55 μm eye-safe range. OSA TOPS 1, 1996: IL4

Acknowledgements This work was supported by the National Natural Science Foundation of China (51722202, 51972118 and 51572023), the Guangdong Provincial Science & Technology Project (2018A050506004), and Innovation Projects of Department of Education of Guangdong Province (2018KQNCX265).

Author contributions Hu T, Xia Z and Zhang Q conceived the project, wrote the paper and were primarily responsible for the experiment. Gao Y carried out photoluminescence measurements and Molokeev M performed the structure refinement. All authors contributed to the general discussion.

Conflict of interest The authors declare that they have no conflict of interest.

Supplementary information Supplementary information is available in the online version of this article.

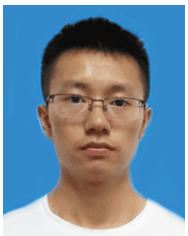

Tao Hu is currently pursuing his PhD degree in the South China University of Technology under the supervision of Prof. Qinyuan Zhang and Prof. Zhiguo Xia. He obtained his master degree from Fujian Normal University in 2018 and joined Prof. Yuansheng Wang's group in Fujian Institute of Research on the Structure of Matter, Chinese Academy of Sciences (CAS) in 2016. His current research interests mainly focus on inorganic luminescent materials for temperature sensing and solid state lighting.

Zhiguo Xia is a professor in the South China University of Technology. He obtained his bachelor degree in 2002 and master degree in 2005 from Beijing Technology and Business University, and received his PhD degree from Tsinghua University in 2008. His research interests include two parts, and one is about the discovery of new rare earth doped solid state materials, and the other one is the discovery of new luminescent perovskite crystals, nanocrystals and their luminescence properties.

Qinyuan Zhang is a professor in the South China University of Technology. He obtained his PhD degree from Shanghai Institute of Optics and Fine Mechanics (SIOM), CAS in 1998. His research interests focus on (1) glass science and technology and (2) rare earth optical materials. He has published more than 200 papers. He was awarded the National Science Fund for Distinguished Young Scholars and "Changjiang Scholar" by Ministry of Education.

$Ca_2Al_2SiO_7$非化学计量调控实现混合价态Eu(+2, +3)应用于比例型温度传感

胡桃[1], 高妍[2], Maxim Molokeev[3,4,5], 夏志国[1*], 张勤远[1*]

摘要 基于不同价态Eu^{2+}/Eu^{3+}的电子结构和电子晶格相互作用的差异，Eu混价共掺杂发光材料在比例型荧光温度传感领域具有应用潜力．本文中，我们制备了具有非化学计量的$Ca_2Al_2Si_{1-x}O_7$:Eu (x = 0.00, 0.02, 0.04)发光材料，基于Si含量的控制，实现了Eu^{2+}和Eu^{3+}的共存与调控，并提出了$2Ca^{2+} + Si^{4+} \longleftrightarrow Eu^{2+} + Eu^{3+} + Al^{3+}$共取代模型，解释了该体系的晶体结构稳定性与电荷平衡机理．得益于Eu^{2+}和Eu^{3+}发光温度依赖差异大，基于$Ca_2Al_2Si_{1-x}O_7$:Eu发光材料的温度探针呈现出良好温敏性能，其最大绝对灵敏度和相对灵敏度分别为0.024 K^{-1}(303 K)和2.46% K^{-1}(443 K)，且信号甄别度高．通过位形坐标曲线分析，揭示了Eu^{2+}发光表现出强烈温度依赖特性的原因，即：Eu^{2+}离子5d能级上的电子易通Eu^{2+}/Eu^{3+}金属-金属电荷迁移带(IVCT)退激发所致．本工作不仅表明$Ca_2Al_2Si_{1-x}O_7$:Eu有望应用于非接触式温度传感，同时也证明了具有混合价态Eu的发光材料在光学测温中的应用．

